Biosensors and Bioelectronics 126 (2019) 838–844

Contents lists available at ScienceDirect

Biosensors and Bioelectronics

journal homepage: www.elsevier.com/locate/bios

Graphene nanogap electrodes in electrical biosensing

Trupti Terse-Thakoor[a,*,1], Pankaj Ramnani[b,2], Claudia Villarreal[c,3], Dong Yan[d,1], Thien-Toan Tran[a,b], Tung Pham[b], Ashok Mulchandani[b,c,**]

[a] Department of Bioengineering, University of California, Riverside, CA 92521, United States
[b] Department of Chemical and Environmental Engineering, University of California, Riverside, CA 92521, United States
[c] Materials Science and Engineering Program, University of California, Riverside, CA 92521, United States
[d] Center for Nanoscale Science and Engineering (CNSE), University of California, Riverside, CA 92521, United States

ARTICLE INFO

Keywords:
Chemical vapor deposition
Graphene
Nanogap electrode
Electrical biosensor

ABSTRACT

Graphene nanogap electrodes are reported here for the first time in an electrical biosensor for the detection of biomolecular interactions. Streptavidin-biotin was chosen as a model system for evaluating the sensor's performance. High-affinity interactions of streptavidin-gold nanoparticles (strep-AuNPs) to the biotin-functionalized nanogap localizes AuNPs, thereby bridging the gap and resulting in changes in device conductance. Biosensing performance was optimized by varying the gap size, AuNP diameter, and streptavidin coverage on AuNPs. The sensitivity and limit of detection (LOD) of streptavidin detection with the optimized parameters were determined to be 0.3 μA/nM and 0.25 pM, respectively. The proposed platform suggests high potential as a portable point-of-use biosensor for the detection of other affinity-based biomolecular interactions, such as antigen-antibody, nucleic acid, or chemo-selective interactions.

1. Introduction

Nanogap electrode as biosensors is a new concept that is rapidly gaining prominence as a powerful platform for ultrasensitive detection of biomolecules. The most salient characteristic of the platform is the direct transduction of the biospecific or chemospecific binding event into an electrical signal, such as resistance/impedance (Lu et al., 2016; Singh et al., 2010), capacitance (Hsueh and Lin, 2016; Mannoor et al., 2010; Yi et al., 2005) or field-effect (Gu et al., 2009; Kim et al., 2009). Additional features include compatibility with semiconductor manufacturing technology, miniaturization, and low cost. Two nanogap electrodes architectures, planar (single or interdigitated) (Singh et al., 2010) and vertical (Jang et al., 2007; Strobel et al., 2007), are generally used in these biosensors. The former is used primarily in devices measuring resistance as a signal while the latter is employed in devices largely measuring capacitance.

Target-probe binding events in the planar gap have been shown previously as a detection method via change in conductivity (Ahn et al., 2011; Cheng et al., 2005; Fang et al., 2008; Kong et al., 2008; Marcon et al., 2007; Park et al., 2002; Tsai et al., 2005; Velev and Kaler, 1999). However, the large gap size (ranging from 300 nm to tens of microns) in the earlier reports limited the sensitivity and limit of detection (LOD) of these sensors. These reports of electrical detection in large gap electrodes commonly use silver deposition post-capture of nanoparticle-tagged target in the gap to enlarge the captured nanoparticle to create a conductive bridge across the insulating nanogap. A detection limit of 50 fM for 22 bases-long DNA (Fang et al., 2008) and 1 pg/ml of human IL5 (Ahn et al., 2011) was realized using 300 nm gap electrodes through aggregates of AuNPs followed by a silver enhancement step catalyzed by the AuNPs on the captured ligand to bridge the gap. Even though promising, the silver enhancement step is time-consuming, costly, complex, and can generate background current from non-target related silver precipitation on gold electrodes. A solution that can alleviate these problems is narrowing the gap size between planar electrodes to less than 100 nm. (Haguet et al., 2004; Marcon et al., 2008a,b). While the reports of electrical biosensors based on gap size less than 100 nm demonstrated that sensing was feasible without silver enhancement, to the best of our knowledge, the important analytical figures of merit of sensitivity and LOD have not been reported. Additionally, a systematic investigation of the interplay between the gap size, AuNP diameter and

* Corresponding author at: Department of Bioengineering, University of California, Riverside, CA 92521, United States.
** Corresponding author at: Department of Chemical and Environmental Engineering, University of California, Riverside, CA 92521, United States.
E-mail addresses: tters001@ucr.edu (T. Terse-Thakoor), adani@engr.ucr.edu (A. Mulchandani).
[1] Department of Electrical and Computer Engineering, Tufts University, Medford, MA 02155, United States.
[2] Lam Research Corporation, Tualatin, OR 97062, United States.
[3] Department of Materials Science and Engineering, Tecnológico de Costa Rica, Cartago 30101, Costa Rica.

https://doi.org/10.1016/j.bios.2018.11.049
Received 17 October 2018; Received in revised form 20 November 2018; Accepted 21 November 2018
Available online 07 December 2018

the surface coverage of analyte, has not been conducted to fully optimize the sensor performance towards the goal of making it an ideal platform for highly sensitive detection.

Graphene is a sp^2 hybridized carbon allotrope with atoms arranged in a honeycomb structure to form a 2D monolayer of graphitic structure analogous to a polycyclic aromatic hydrocarbon of quasi-infinite size (Fitzer et al., 1995). It has become an attractive material in the development of electrochemical/electrical biosensor devices due to its excellent electrical, chemical, and mechanical properties, which include large surface area per unit weight, high charge carrier concentrations, and exceptional electron mobility. Owing to its two-dimensional structure, graphene is an ideal material for creating atomically thin nanogaps of width down to the dimension of a single molecule compared to more bulky metal electrodes (Prins et al., 2011). Carbon nanotubes (CNTs) are also suitable for making atomically thin nanogaps, but the ease of device fabrication using large area chemical-vapor-deposition-grown (CVD) graphene makes it more favorable (Kong et al., 1998). Additionally, we hypothesize that such atomically thin graphene (thickness ~0.33 nm) nanogap electrodes would allow us to capture AuNPs of size greater than the gap width while maintaining the biospecific interaction of analyte compared to metal nanogap electrodes of thickness of 20–200 nm (Kim et al., 2009; Marcon et al., 2008a,b). As a result, only a small number of AuNPs is required to bridge the nanogap, which in turn yields a higher sensitivity.

Graphene-based planar nanogap electrodes have been previously fabricated using methods such as feedback controlled electroburning (Prins et al., 2011) and divulsion (Wang et al., 2010) for applications in molecular electronics. There are also different methods reported which can be potentially used to make graphene nanogap electrodes such as atomic force microscopy (AFM) lithography (Lu et al., 2010), electrical breakdown of graphene sheets (Standley et al., 2008), and anisotropic etching of graphene using metallic nanoparticles (Datta et al., 2008). Even though these methods are promising in fabricating nanogaps with widths varying between less than 20 nm to few nanometers, they experience several limitations in terms of reproducibility and producing well-defined patterns. In our work, reproducibility and uniformity of nanogaps are crucial because our biosensor involves the capture of AuNPs of well-defined sizes across the nanogap. Owing to these reasons, we have studied three different methods of nanogap fabrication including focused ion beam milling (FIB), nanoindentation, and electron-beam lithography (EBL) to produce reproducible and uniform gap size of less than 100 nm. FIB and EBL methods have been reported in the literature for patterning graphene such as making graphene nanoribbons (Abbas et al., 2014; Chen et al., 2007; Tan et al., 2013). However, nanoindenter has not been investigated for patterning graphene nanostructure. Nanoindentation is otherwise a common technique used in testing the mechanical properties of materials such as modulus of elasticity, hardness, yield strength, fracture toughness, scratch hardness, and wear properties, including that of graphene and graphene composites (Han et al., 2016; King et al., 2015; Kumar et al., 2016; Martinez-Asencio et al., 2016; Suk et al., 2015).

We report, a proof-of-concept study where highly conductive, monolayer graphene is used as an electrode material for nanogap electrodes for electrical biosensing using AuNPs. We fabricated reproducible graphene nanogap electrodes using a combination of photolithography (PL) and EBL. The streptavidin-biotin interaction was chosen as a model system for evaluating the graphene nanogap sensor's performance. We also investigated the interplay of the gap size, AuNP diameter and protein coverage on the AuNP in the device. This simple electrical transduction-based biosensor platform has great potential as a portable point-of-care/use device with a handheld multimeter.

2. Experimental

2.1. Materials

Strepatavidin-labeled gold nanoparticles (strep-AuNPs) solution (25 μg streptavidin per ml of AuNP) of 10 and 60 nm diameter containing 2.8×10^{13} nanoparticles/ml and 2.3×10^{11} nanoparticles/ml, respectively, were purchased from Nanocs, Inc. (Boston, MA, USA). In-house AuNPs for bioconjugation of streptavidin were synthesized using sodium citrate reduction method (Storhoff et al., 1998). Biotinamidohexanoic acid N-hydroxysuccinimide ester (Biotin-LC NHS) was purchased from Sigma-Aldrich (St. Louis, MO, USA). Sodium phosphate buffer (PB) 50 mM of pH 7.4 was used as incubation buffer and PB with 0.5% Tween 20 (PBT), PB with 1% bovine serum albumin (PBA) or PB with 0.5% Tween 20% and 1% BSA (PBTA) was used as the blocking buffer. All organic solvents were of analytical grades and purchased from Fischer Scientific (Hampton, NH, USA). Water used in the sensing experiments is purified using Milli-Q purification system (Millipore, Burlington, MA, USA).

2.2. Instruments

Graphene was grown by CVD using a tube furnace (Lindberg/Blue, Mini-Mite, Thermo Scientific, USA). A Suss MicroTech mask aligner (Model MA6, SÜSS MicroTec SE, Garching, Germany) was used for standard photolithographic patterning of microelectrodes followed by deposition of metal contact pads using an e-beam evaporator (Temescal BJD-1800, Temescal, Livermore, CA, USA). A Leo SUPRA 55 (Thornwood, NY, USA) was employed for EBL and a Leo XB1540 (Thornwood, NY, USA) was used for FIB. A Hysitron Inc. TI-950 triboindenter (Billerica, MA, USA) was used for nanoindentation of graphene. Electrical measurements were performed using a semiconductor parameter analyzer (HP Agilent 4156B, CA, USA). Scanning electron microscopy (SEM) images were obtained on a Philips XL30-FEG system (Hillsboro, OR, USA).

2.3. Graphene synthesis and transfer

Graphene was synthesized by CVD method using copper (Cu) foil (99.98% purity, 25 μm thickness) as a substrate for growth. Cu foil was sequentially cleaned in 10% acetic acid, deionized water, acetone, and isopropanol (IPA) for 10 min/each to remove any oxide and organic impurities. The Cu foil was dried under nitrogen gas, placed inside a fused silica tube (5 cm inside diameter × 100 cm long) and annealed for 2 h at 1030 °C under a flowing mixture of Argon (Ar) at 300 sccm and hydrogen (H_2) at 15 sccm at atmospheric pressure. For growth of graphene, diluted methane (CH_4) (90 ppm in Ar) at 350 sccm and H_2 were supplied for 26 min. In the final step, CH_4 flow was turned off and the furnace was cooled to room temperature by flowing Ar and H_2.

To transfer graphene from the Cu foil to silicon dioxide/silicon (SiO_2/Si) substrate, poly (methyl methacrylate) (PMMA) 950 KA4 solution was spin coated onto the graphene/Cu foil and baked at 60 °C for 10 min. The PMMA/graphene/Cu foil was then cut into desired size pieces and Cu was etched in 0.3 M ferric chloride ($FeCl_3$) solution. The resulting PMMA/graphene film floating on $FeCl_3$ solution was cleaned with aqueous hydrochloric acid (HCl, 5%) followed by deionized water to ensure no copper or $FeCl_3$ traces were left. Finally, the PMMA/graphene film was transferred to a SiO_2/Si substrate followed by sequential drying in air and in an oven at 50 °C for 1 h. To remove the PMMA from the graphene a drop of fresh PMMA solution was placed on the PMMA/graphene film for 1 min, thinned out by spinning at 3000 rpm for 30 s and finally dipped in an acetone bath at 60 °C.

2.4. Fabrication of graphene microelectrodes

Channel regions with dimensions of $L_c = W_c = 10$ μm were defined

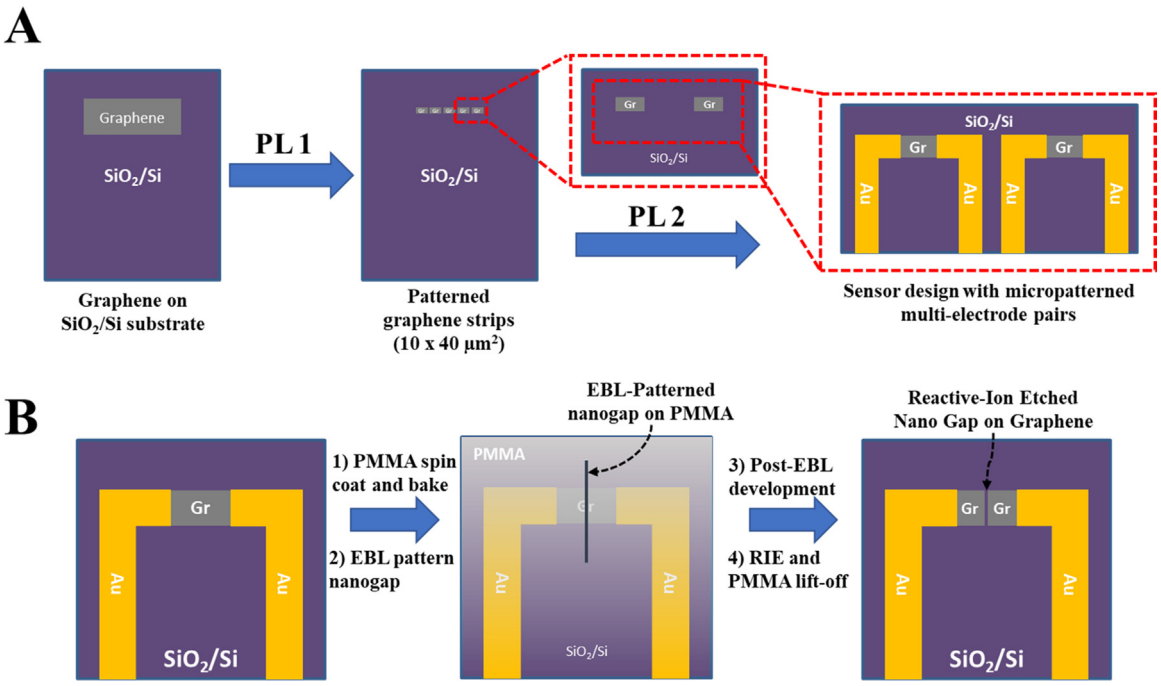

Fig. 1. A) Schematic of the photolithographic writing of the planar micropatterned graphene electrodes and B) Schematic for planar nanogap electrode fabrication.

in graphene on SiO_2/Si substrate using standard photolithography (PL1), followed by oxygen-based reactive ion etching (O_2-RIE). Contact pads were patterned using a second photolithography step (PL2), followed by deposition of 20/120 nm layer of Cr/Au using e-beam evaporation and lift-off. Fig. 1A illustrates the fabrication process for planar graphene electrodes.

2.5. Nanogap fabrication

Graphene microelectrodes were cleaned with acetone and IPA followed by drying with nitrogen gas. The EBL resist, i.e. PMMA 950 KA4, was spin coated onto the chips in two steps, step I: 1000 rpm at the ramp of 300 rpm/s for 3 s and step II: 5000 rpm at the ramp of 1000 rpm/s for 45 s. The chips were then baked at 180 °C for 30 min. A line pattern was fabricated in the center of the graphene electrode by EBL writing (20 keV, varying beam current and electron dose). The line pattern transferred on the PMMA was developed using 1:3 solution of MIBK: IPA (MIBK – methyl isobutyl ketone, IPA – isopropyl alcohol) solvent for 70–90 s. The exposed graphene in the line pattern was removed using O_2-RIE. Finally, PMMA was removed by immersing in and washing the chip with acetone. A schematic of nanogap fabrication by EBL is shown in Fig. 1B.

2.6. Functionalization of nanogap with biotin

During initial experiments, the nanogap space of SiO_2 substrate between the pair of graphene electrodes was treated with piranha solution (sulfuric acid: hydrogen peroxide, 5:1) for 30 min and washed thoroughly with water. The hydrophilic SiO_2 surface was then modified with a self-assembled monolayer (SAM) of 3-aminopropyl triethoxysilane (APTES) by incubating the chips in APTES solution for 1 h followed by washing with water and drying by flowing N_2. A 10 mM Biotin-LC NHS solution in dimethylformamide (DMF) was drop-casted (5 µL) to cover the electrode area and incubated for an hour. Chips were then washed with water, dried gently by blowing nitrogen and incubated with aqueous PBT for 30 min to block nonspecific adsorption of strep-AuNPs on the graphene surface and then thoroughly washed with water and buffer.

Based on the observations (discussion section) of initial experiments with above method of biotin functionalization, an alternative functionalization protocol was used in the later experiments. In this modified protocol, after EBL development and O_2-RIE step (before PMMA lift-off), an additional step of plasma ashing for 30 s at 100 W was performed. Plasma ashing is used to activate SiO_2 in the nanogap for efficient functionalization with APTES instead of piranha treatment. After APTES treatment, the chip was washed with acetone to remove PMMA resist protecting graphene electrodes. For better passivation of graphene, PBTA solution was used. Schematics of original and modified protocol for nanogap functionalization are shown in Figs. S1A and S1B, respectively.

2.7. Biosensing of strep-AuNP

Chips were incubated for 1 h with 2 µL of each dilution of strep-AuNP, washed with PB buffer followed by water, and dried gently with N_2. Electrical measurements were performed before and after strep-AuNP incubation using a semiconductor parameter analyzer (HP Agilent 4156B) by sweeping the potential from −5 to +5 V with 50 mV steps. Fig. S1C illustrates a schematic of strep-AuNP capture on the chip.

2.8. Optimization of biosensor performance

The nanogap biosensor performance was optimized by varying the gap size, AuNPs diameter, and protein coverage on AuNPs. The sensing performance was measured in terms of the lowest concentration of streptavidin on AuNPs that first bridge the gap (LCFB), resulting in conductance change. The gap size of 30 and 60 nm with strep-AuNP of 10 and 60 nm diameter were used in the testing. To vary the protein coverage on AuNPs, streptavidin conjugation was carried out using passive adsorption method. Streptavidin needed for 100% coverage of each size AuNP was first determined using sodium chloride titration method (Thobhani et al., 2010). Based on protein required for 100% coverage, different dilutions of streptavidin solutions were then incubated with AuNPs dispersion in PB for 30 min at room temperature. The unbound streptavidin was determined from the supernatant and buffer washings, by measuring the absorbance (at 280 nm). Protein coverage on AuNPs was estimated based on the bound streptavidin

concentration and AuNPs density. Amount of streptavidin required for 10%, 25%, and 40% coverages were then incubated with AuNPs solution and unfunctionalized surfaces on the AuNPs were further blocked by incubating it with BSA (1%) solution in PB overnight at 4 °C. This mixture was then centrifuged to collect the strep-AuNPs, followed by two buffer washings to remove any unbound protein and finally dispersed in known volume of buffer. Different dilutions of respective coverage strep-AuNP were incubated on the biotin functionalized chips for measuring LCFB values.

3. Results and discussion

3.1. Fabrication of graphene nanogap electrode

We investigated three different methods of fabricating planar nanogap of less than 100 nm in graphene. These methods were namely, focused Ga^+-ion beam milling, nanoindentation, and EBL. When compared to EBL, FIB, and nanoindentation methods are resist free. Our goal was to find a method that can reproducibly make less than 100 nm sized nanogaps without affecting graphene properties and result in a device suitable for detecting the biomolecular interaction at the nanoscale. Based on the ability of the three methods to make reproducible nanogaps combined with their pros and cons summarized in Table S2 (see Supplementary Information), we selected the EBL as the method for making nanogap graphene electrodes for further work. Details of experimental methods and results for FIB and nanoindentation to make graphene nanogap electrodes are provided in the Supplementary Information (Table S1, Figs. S2 and S3).

In EBL optimization, for patterning the nanogap in graphene film, first, the resist thickness and baking time was set to 180 nm and 30 min, respectively. Experiments with a higher thickness of up to 350 nm and baking time of 2 h, as reported for sub 100 nm patterns on SiO_2 using EBL (Chen et al., 2006), resulted in non-continuous line pattern across graphene electrode. On the other hand, resist thickness less than 180 nm was found to be too thin, such that PMMA was overexposed even during pattern alignment and damaged the graphene. Next, the beam current, line dose, and aperture size were varied. Varying the combination of line dose and beam current (Fig. 2) and aperture size (Fig. 3A) resulted in nanogap width of 400 nm to ~34 nm. I-V curves after O_2-RIE of graphene in the developed line pattern exhibited the desired high resistance, confirming a clean gap formation (Fig. 3B).

3.2. Electrical biosensing using graphene nanogap electrode

The principle of electrical detection of streptavidin in the proposed biosensor is based on the electrical current/conductivity change associated with the bridging of the nanogap between two planar electrodes by metallic nanoparticle(s). This bridging event occurs as a result of biospecific binding of streptavidin captured on AuNP to the biotin immobilized within the nanogap.

Graphene nanogap with 65 nm gap width and commercial strep–AuNP of 10 nm diameter was first tested. A chip with five pairs of electrodes, which consists 65 nm gap in each, were incubated with ten times diluted strep-AuNP of 10 nm followed by measuring the current (I) when the potential (V) was scanned from +5 to −5 V and SEM observation. I-V curve was measured after biotin functionalization and blocking step (original method as described in experimental section) and then after incubation with strep-AuNP. As illustrated in Fig. 4A, the current measured after blocking step (without strep-AuNP) over the full potential window was less than 10^{-9} A, attributed to background current. This background current varies from chip to chip between 10^{-9} to 10^{-13} A depending upon the uniformity of SiO_2 grown on Si wafers, resulting in varied leakage current. With the subsequent incubation with strep-AuNP, the current increased to 10^{-7} A due to the capture of strep-AuNP (Fig. 4A) at a threshold voltage of ± 1 V. A non-linear I-V (S-shaped) curve is attributed to the presence of AuNP in the nanogap (Marcon et al., 2008b). In contrast, there was no change in current when just PB was incubated with biotin functionalized nanogaps (negative controls) and also when strep-AuNPs were incubated with nanogaps without biotin (positive controls; data not shown). This corroborates that the strep-AuNP were selectively captured in the biotin functionalized nanogap area. Next, we investigated the I-V response (Fig. 4C) when the different concentration of strep-AuNPs (10 nm) was applied to the nanogap electrode (65 nm gap width).

As can be seen in I-V curve in Fig. 4C, the LCFB for 10 nm strep-AuNPs and 65 nm gap width is 0.95 μM. Such high LCFB clearly indicates that large number of 10 nm AuNPs are required to bridge the large gap width (65 nm). Once the gap is bridged, the current increased with further incubations with higher concentration but as most of binding sites are already occupied by AuNPs at such high LCFB, the current increase with increasing concentrations is not perfectly linear. High LCFB with 10 nm AuNP with 65 nm gap width, was the motivation to study the effect of gap width and AuNPs size on LCFB.

As seen in Fig. 4B, the strep-AuNP were captured not only in the nanogap, but also on the graphene electrodes which also contributed to high LCFB. We hypothesize this is due to the formation of graphene oxide during piranha treatment, which creates the active sites for chemical bonding to APTES and in turn leads to attachment of Biotin-LC-NHS. In order to alleviate oxidation of graphene, we replaced piranha treatment step with plasma ashing followed by a treatment with PBTA after APTES and Biotin-LC-NHS functionalization to effectively prevent nonspecific binding of strep-AuNP to graphene. As shown in Fig. 5, the modified method significantly reduced strep-AuNP binding on the graphene electrodes.

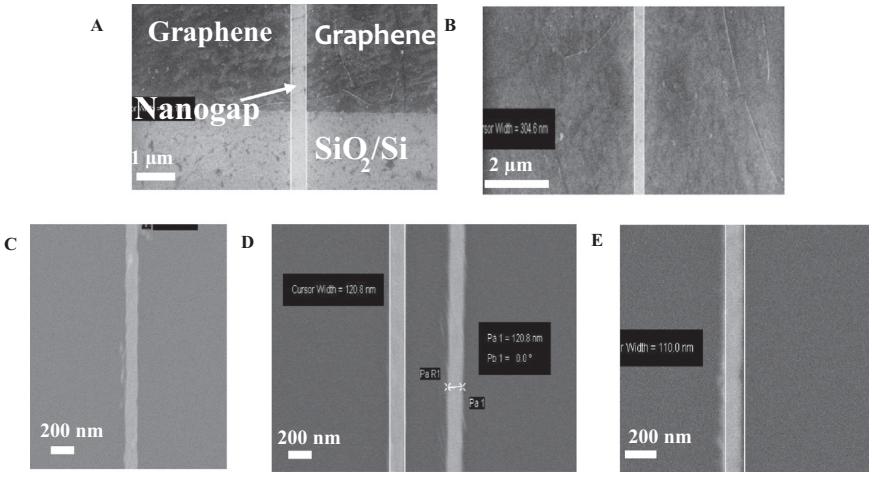

Fig. 2. SEM images showing different gap widths (in nm) obtained from varying beam current (in pA) and line dose (in nC/cm). A) 408 nm using 70 pA and 6 nC/cm, B) 304 nm using 65 pA and 4 nC/cm, C) 132 nm using 20 pA and 2 nC/cm, D) 121 nm using 1.75 nC/cm, E) 110 nm using 20 pA and 1.5 nC/cm. A and B shows SEM images of nanogaps after O_2-RIE of graphene in the nanogap whereas C, D and E are SEM images of nanogaps with metal deposited in the nanogap for better visualization.

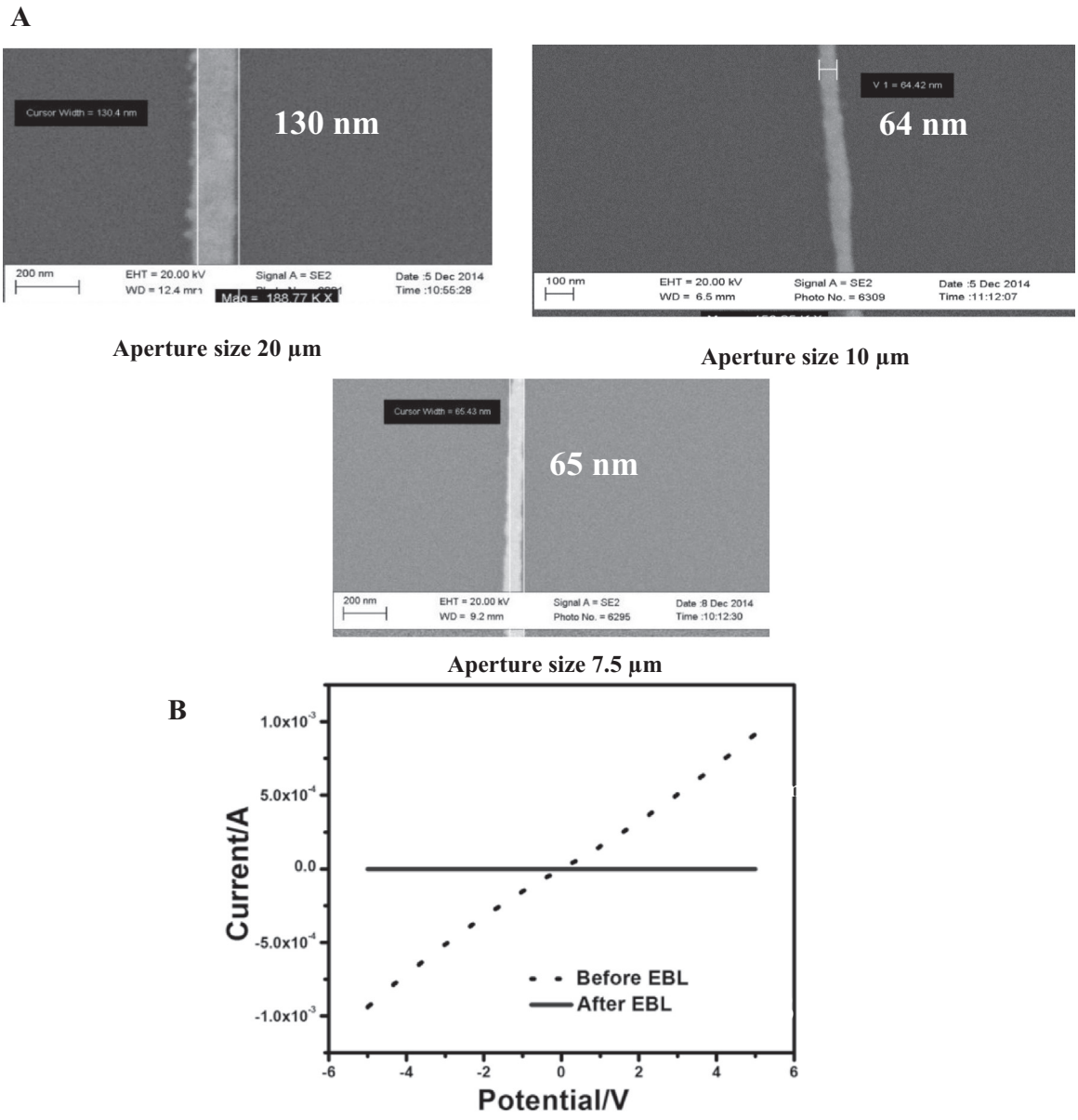

Fig. 3. A) SEM images showing the effect of aperture size on gap width (in nm) at beam current and line dose of 20 pA and 2 nC/cm, respectively. B) I-V curve of graphene electrode before and after nanogap (width of 65 nm) by EBL.

3.3. Optimization of biosensor performance

The response and, in-turn, the sensitivity and LOD of the present nanogap biosensor are inter-dependent on the size of nanogap and size and streptavidin coverage of AuNP. To study this interdependency, we first determined LCFB for nanogap sizes of 30 and 65 nm using AuNPs of 10 and 60 nm with 20% coverage on chips functionalized with modified method and better passivation. The results are summarized in Table 1. Fig. 5 shows the capture of 60 nm of strep-AuNP across 30 nm and 65 nm of gap width. The results show that for a constant strep-AuNP size, LCFB was lower for smaller nanogap, whereas for a constant nanogap size, LCFB was lower for larger strep-AuNP. Furthermore, the lowest LCFB was obtained for smaller nanogap (30 nm) and larger AuNP (60 nm). This shows that a smaller gap width and larger AuNP size leads to a fewer number of AuNPs required to bridge the gap and resulted in the lowest LCFB. This also proves our hypothesis that use of atomically thin graphene (~0.33 nm) as an electrode material is crucial in allowing efficient binding of analyte coated larger AuNP to its receptor in the nanogap without any hindrance from thickness/height of the electrode (Fig. 5B).

Based on our other hypothesis that streptavidin coverage (number of streptavidin molecules) on the AuNPs will be crucial for LCFB, we investigated the effect of streptavidin surface coverage (10%, 20% and 40%) on AuNP of 10 and 60 nm and nanogap width of 30 and 60 nm on LCFB. The LCFB data for 10% covered 10 nm and 60 nm AuNP is not included in the table as they failed to bridge the gap. This might have resulted from scarcity of streptavidin molecules on the AuNP surface, as well as the available number of strep-AuNP (needed for bridging the gap) that could not come in the vicinity of biotin for binding in stipulated incubation time of 1 h. As shown in Table 2, the lowest LCFB (0.24 nM) was attained for the combination of 20% streptavidin coverage on AuNP of 60 nm with graphene electrode gap size of 30 nm.

Analytical characterization was carried out for the optimized combination of gap size (30 nm), and strep-AuNP size (60 nm) and protein coverage (20%) by measuring response with increasing concentration/number of strep-AuNP (Fig. 6). Sensitivity and LOD of streptavidin detection with optimized parameters were found to be 0.3 µA/nM and 0.25 pM, respectively. LOD is estimated using the relationship of

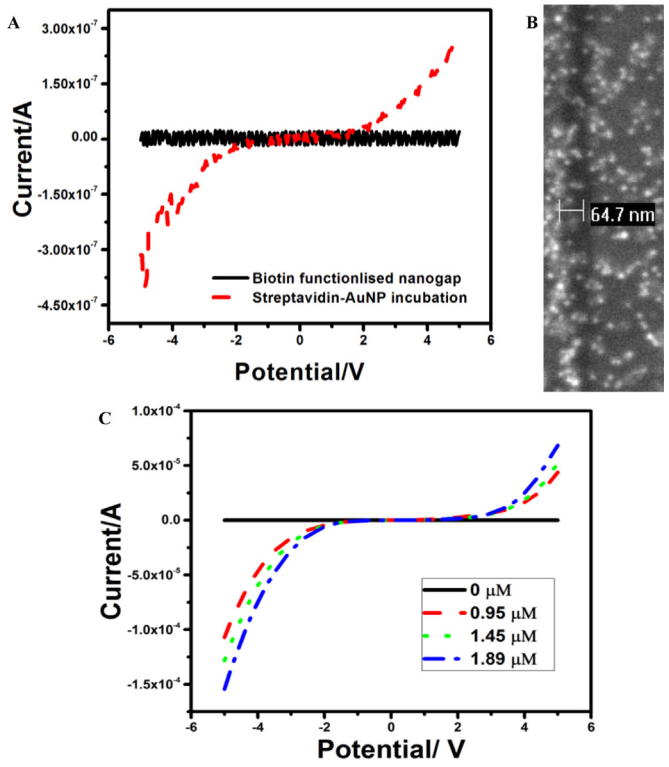

Fig. 4. A) I- V curve with biotin functionalized and after incubation with strep-AuNP. B) SEM image of nanogap with captured strep-AuNP. C) I-V curves after incubation with different concentration of strep-AuNP.

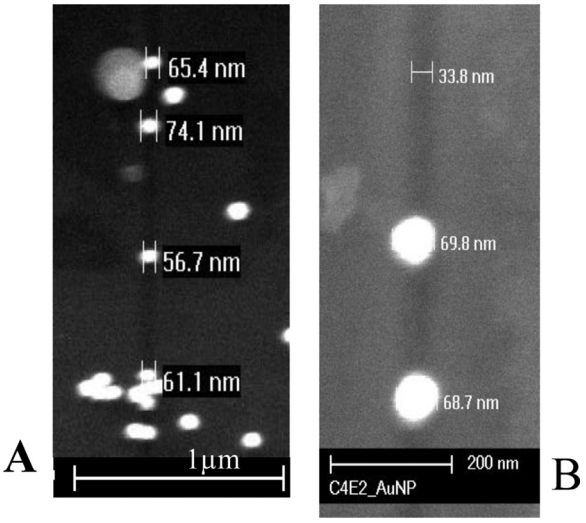

Fig. 5. SEM images showing capture of strep-AuNP (~60 nm) across gap width of A) 65 nm and B) ~30 nm.

Table 1
Effect of gap size and AuNP diameter on LCFB at streptavidin coverage of 20%.

Parameter combinations	Gap size (nm)	AuNP diameter (nm)	LCFB (nM)
1	65	10	97
2	30	10	19
3	65	60	64
4	30	60	0.24

Table 2
Compilation of nanogap sensor parameters studied and their LCFB.

Gap size (nm)	AuNP size (nm)	Streptavidin coverage (%)	LCFB (nM)
65	10	20	97
65	10	40	424
65	60	20	64
65	60	40	121
30	10	20	19
30	10	40	42
30	**60**	**20**	**0.24**
30	60	40	4.3

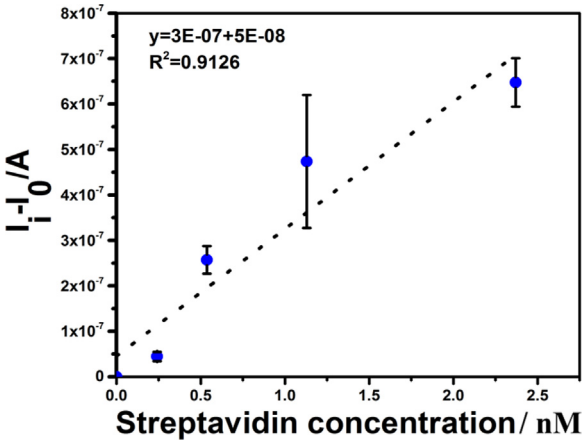

Fig. 6. Calibration plot for optimized combination i.e. 30 nm gap width, 60 nm strep-AuNP with 20% coverage. The data points are average measurements of 5 electrodes and error bar represents ± 1 standard deviation.

LOD = (3 × SD)/m where SD is the standard deviation of blank and m is the sensitivity of the sensor, i.e. slope of the calibration plot. These results are better than previously reported detection of streptavidin using streptavidin-biotin interaction, including amperometric biosensors using metallic nanocube augmented CNT network (Claussen et al., 2009) (LOD of 2.3 nM), ELISA (Lakshmipriya et al., 2016) (LOD of 0.25 nM), ZnO nanorod-based FET (Kim et al., 2006) (LOD of 25 nM), and single-walled CNT thin film transistor (Lamberti et al., 2014) (LOD of 0.1 nM). We are optimistic that performance of the proposed nanogap biosensor can be further improved using nanogap width of less than 30 nm. Our group will also work on exploring this platform in the detection of a single analyte coated nanoparticle from complex samples using multi-electrode array-based chip design.

4. Conclusion

For the first time, graphene nanogap based electrical biosensing platform was successfully developed, tested with their analytical characterization in terms of sensitivity (0.3 μA/nM) and LOD (0.25 pM). Graphene nanogaps fabricated using EBL were reproducible without affecting the graphene properties compared to FIB and nanoindentation. We also established the interdependency between gap size, AuNP diameter, and protein coverage, in developing a high sensitivity electrical biosensor platform. With AuNPs larger than the gap width, optimum analyte coverage on AuNPs and monoatomic thin graphene as an electrode material, we obtained the lowest limit of detection. This biosensor platform has the potential for use as a portable point-of-care/use device in areas where high sensitivity detection is crucial, such as clinical diagnosis, environmental monitoring or even food monitoring.

Acknowledgment

This work was supported by grants from the United States

Department of Agriculture (2014-67021-21589) and the National Science Foundation, United states (1606181) to AM. The authors are thankful to Dr. Xiadong Zhou from the Wuhan University, China for help with the AuNPs synthesis and Prof. David Kisailus from the UC Riverside, USA and his graduate student Mr. Steven Herrera for Nanoindentation instrument. TT acknowledges Ms. Rachel E. Owyeung, a graduate student at Tufts University for checking the manuscript for English writing. We also acknowledge the UCR Central Facility for Advanced Microscopy and Microanalysis for scanning microscopy and Center for Nanoscale Science and Engineering for nanofabrication cleanroom facilities. AM acknowledges the W. Ruel Johnson Chair support.

Appendix A. Supporting information

Supplementary data associated with this article can be found in the online version at doi:10.1016/j.bios.2018.11.049.

References

Abbas, A.N., Liu, G., Liu, B., Zhang, L., Liu, H., Ohlberg, D., Wu, W., Zhou, C., 2014. ACS Nano 8 (2), 1538–1546.
Ahn, J., Lee, T.H., Li, T., Heo, K., Hong, S., Ko, J., Kim, Y., Shin, Y.B., Kim, M.G., 2011. Biosens. Bioelectron. 26 (12), 4690–4696.
Chen, A., Chua, S.J., Chen, P., Chen, X.Y., Jian, L.K., 2006. Nanotechnology 17 (15), 3903–3908.
Chen, Z.H., Lin, Y.M., Rooks, M.J., Avouris, P., 2007. Phys. E Low. Dimens. Syst. Nanostruct. 40 (2), 228–232.
Cheng, Y.-T., Pun, C.-C., Tsai, C.-Y., Chen, P.-H., 2005. Sens. Actuator B Chem. 109 (2), 249–255.
Claussen, J.C., Franklin, A.D., Ul Haque, A., Porterfield, D.M., Fisher, T.S., 2009. ACS Nano. 3 (1), 37–44.
Datta, S.S., Strachan, D.R., Khamis, S.M., Johnson, A.T.C., 2008. Nano Lett. 8 (7), 1912–1915.
Fang, C., Fan, Y., Kong, J.M., Gao, Z.Q., Balasubramanian, N., 2008. Anal. Chem. 80 (24), 9387–9394.
Fitzer, E., Kochling, K.H., Boehm, H.P., Marsh, H., 1995. Pure Appl. Chem. 67 (3), 473–506.
Gu, B., Park, T.J., Ahn, J.H., Huang, X.J., Lee, S.Y., Choi, Y.K., 2009. Small 5 (21), 2407–2412.
Haguet, V., Martin, D., Marcon, L., Heim, T., Stievenard, D., Olivier, C., El-Mahdi, O., Melnyk, O., 2004. Appl. Phys. Lett. 84 (7), 1213–1215.
Han, J., Ryu, S., Kim, D.K., Woo, W., Sohn, D., 2016. EPL 114 (6), 68001.
Hsueh, H.T., Lin, C.T., 2016. Biosens. Bioelectron. 79, 636–643.
Jang, D.Y., Kim, Y.P., Kim, H.S., Park, S.H.K., Choi, S.Y., Choi, Y.K., 2007. J. Vac. Sci. Technol. B 25 (2), 443–447.
Kim, J.S., Il Park, W., Lee, C.H., Yi, G.C., 2006. J. Korean Phys. Soc. 49 (4), 1635–1639.
Kim, S.K., Cho, H., Park, H.J., Kwon, D., Lee, J.M., Chung, B.H., 2009. Nanotechnology 20 (45), 455502.
King, J.A., Klimek, D.R., Miskioglu, I., Odegard, G.M., 2015. J. Compos. Mater. 49 (6), 659–668.
Kong, J.M., Zhang, H., Chen, X.T., Balasubramanian, N., Kwong, D.L., 2008. Biosens. Bioelectron. 24 (4), 787–791.
Kong, J., Soh, H.T., Cassell, A.M., Quate, C.F., Dai, H.J., 1998. Nature 395. pp. 878–881.
Kumar, D., Singh, K., Verma, V., Bhatti, H.S., 2016. J. Nanosci. Nanotechnol. 16 (6), 6400–6406.
Lakshmipriya, T., Gopinath, S.C.B., Tang, T.H., 2016. PLoS One 11 (3), e0151153.
Lamberti, P., Mousavi, S.A., Tucci, V., Wagner V., 2014. IEEE Proceedings of the 9th Nanotechnology Materials and Devices Conference (NMDC), Aci Castello.140–144.
Lu, Y., Guo, Z., Song, J.-J., Huang, Q.-A., Zhu, S.-W., Huang, X.-J., Wei, Y., 2016. Anal. Chim. Acta 905, 58–65.
Lu, G., Zhou, X.Z., Li, H., Yin, Z.Y., Li, B., Huang, L., Boey, F., Zhang, H., 2010. Langmuir 26 (9), 6164–6166.
Mannoor, M.S., James, T., Ivanov, D.V., Beadling, L., Braunlin, W., 2010. Biophys. J. 98 (4), 724–732.
Marcon, L., Stievenard, D., Melnyk, O., 2007. Biosens. Bioelectron. 23 (1), 81–87.
Marcon, L., Melnyk, O., Stievenard, D., 2008a. Biosens. Bioelectron. 23 (7), 1185–1188.
Marcon, L., Stievenard, D., Melnyk, O., 2008b. J. Pept. Sci. 14 (8) (134-134).
Martinez-Asencio, J., Ruestes, C.J., Bringa, E.M., Caturla, M.J., 2016. Phys. Chem. Chem. Phys. 18 (20), 13897–13903.
Park, S.J., Taton, T.A., Mirkin, C.A., 2002. Science 295 (5559), 1503–1506.
Prins, F., Barreiro, A., Ruitenberg, J.W., Seldenthuis, J.S., Aliaga-Alcalde, N., Vandersypen, L.M.K., van der Zant, H.S.J., 2011. Nano Lett. 11 (11), 4607–4611.
Singh, K.V., Whited, A.M., Ragineni, Y., Barrett, T.W., King, J., Solanki, R., 2010. Anal. Bioanal. Chem. 397 (4), 1493–1502.
Standley, B., Bao, W.Z., Zhang, H., Bruck, J., Lau, C.N., Bockrath, M., 2008. Nano Lett. 8 (10), 3345–3349.
Storhoff, J.J., Elghanian, R., Mucic, R.C., Mirkin, C.A., Letsinger, R.L., 1998. J. Am. Chem. Soc. 120 (9), 1959–1964.
Strobel, S., Arinaga, K., Hansen, A., Tornow, M., 2007. Nanotechnology 18 (29).
Suk, J.W., Mancevski, V., Hao, Y.F., Liechti, K.M., Ruoff, R.S., 2015. Phys. Status Solidi Rapid Res. Lett. 9 (10), 564–569.
Tan, X.B., Chuang, H.J., Lin, M.W., Zhou, Z.X., Cheng, M.M.C., 2013. J. Phys. Chem. C 117 (51), 27155–27160.
Thobhani, S., Attree, S., Boyd, R., Kumarswami, N., Noble, J., Szymanski, M., Porter, R.A., 2010. J. Immunol. Methods 356 (1–2), 60–69.
Tsai, C.Y., Chang, T.L., Uppala, R., Chen, C.C., Ko, F.H., Chen, P.H., 2005. Jpn. J. Appl. Phys. 44 (7B), 5711–5716.
Velev, O.D., Kaler, E.W., 1999. Langmuir 15 (11), 3693–3698.
Wang, H.M., Zheng, Z., Wang, Y.Y., Qiu, J.J., Guo, Z.B., Shen, Z.X., Yu, T., 2010. Appl. Phys. Lett. 96 (2), 023106.
Yi, M.Q., Jeong, K.H., Lee, L.P., 2005. Biosens. Bioelectron. 20 (7), 1320–1326.